AJNR

Magnetization transfer or spin-lock? An investigation of off-resonance saturation pulse imaging with varying frequency offsets.

J L Ulmer, V P Mathews, C A Hamilton, A D Elster and P R Moran

AJNR Am J Neuroradiol 1996, 17 (5) 805-819
http://www.ajnr.org/content/17/5/805

Magnetization Transfer or Spin-Lock? An Investigation of Off-Resonance Saturation Pulse Imaging with Varying Frequency Offsets

John L. Ulmer, Vincent P. Mathews, Craig A. Hamilton, Allen D. Elster, and Paul R. Moran

PURPOSE: To characterize near-resonance saturation pulse MR imaging on a 1.5-T scanner in order to gain insight into underlying mechanisms that alter tissue contrast and to optimize the technique for neuroimaging. **METHODS:** Off-resonance saturation pulses were applied to T1-weighted, spin-density-weighted, and T2-weighted sequences at frequency offsets ranging from 50 Hz to 20 000 Hz down field from water resonance. Suppression ratios were determined at each offset for phantom materials ($MnCl_2$ solution, gadopentetate dimeglumine, corn oil, water, and agar), normal brain structures, and a variety of brain lesions. **RESULTS:** Signal suppression of $MnCl_2$ on T1-weighted images occurred at offsets of less than 2000 Hz even though no macromolecules were present in the solution. Only those phantom materials and tissues with short or intermediate T1 relaxation times and relatively large T1/T2 ratios were sensitive to changing frequency offsets. Suppression of brain increased from approximately 20% at 2000 Hz offset to approximately 45% when the offset was reduced to 300 Hz. In human subjects, the net effect of reducing the frequency offset was to increase T2 contrast on T1-weighted, spin-density-weighted, and T2-weighted images. Distilled water and contrast material did not suppress except at very low offsets (<300 Hz). A frequency offset of 300 Hz was optimal for maximizing conspicuity between most contrast-enhancing lesions and adjacent brain while preserving anatomic detail. **CONCLUSION:** Suppression of $MnCl_2$ indicates that magnetization transfer is not the sole mechanism of contrast in near-resonance saturation MR imaging. Spin-lock excitation can reasonably explain the behavior of the phantom solutions and the increase in T2 contrast of tissues achieved as the frequency offset is decreased from 2000 Hz to 300 Hz. Below 300 Hz, saturation is presumably caused by spin-tip effects. With our pulse design, an offset of 300 Hz is optimal for many routine clinical imaging examinations.

Index terms: Magnetic resonance, experimental; Magnetic resonance, magnetization transfer

AJNR Am J Neuroradiol 17:805–819, May 1996

Off-resonance saturation pulse imaging is a relatively new magnetic resonance (MR) imaging technique that selectively suppresses and alters the contrast of normal and abnormal brain tissues (1). The technique applies a preparatory radio frequency pulse at a specific frequency offset from water resonance (near 1000 Hz for most commercially available systems) before a standard imaging sequence. Off-resonance imaging has already proved useful in a number of neuroimaging applications: for improving visibility of small vessels in time-of-flight MR angiography (2, 3), for detecting cerebral infarction (4–7), for displaying the internal structure of the eye (8), for assessing disorders of myelin (6, 9–11), for evaluating infections of the central nervous system (6, 7), and for characterizing a variety of intracranial mass lesions (6, 7, 12, 13). According to current theory, an off-resonance radio frequency pulse selectively saturates the pool of macro-

Received September 7, 1995; accepted after revision January 8, 1996.

Dr Ulmer received the Cornelius G. Dyke Memorial Award for this paper at the annual meeting of the American Society of Neuroradiology, Chicago, Ill, April 1995.

From the Department of Radiology, Bowman Gray School of Medicine, Winston-Salem, NC.

Address reprint requests to John L. Ulmer, MD, Department of Radiology, Medical College of Wisconsin, 9200 W Wisconsin Ave, Milwaukee, WI 53226.

AJNR 17:805–819, May 191996 0195-6108/1996/1705–0805

molecular protons and affects tissue contrast by a mechanism known as magnetization transfer (MT) (1, 14–16). MT saturation of the macromolecular pool modulates MR signal from the nearby water molecules, presumably by means of dipolar cross-coupling and chemical exchange interactions.

Several methods of off-resonance saturation imaging have been used in clinical studies, including continuous wave irradiation and pulsed techniques (1, 17–19). Because of specific absorption rate constraints, continuous wave methods used in low-field experiments have been largely replaced with off-resonance pulsed methods for clinical use on high-field systems. Although considerable research has documented the effects of MT in this setting, much of the theory concerning contrast generation remains speculative, and other mechanisms may be involved in the signal modulation. In fact, when preparatory pulses are applied within several thousand Hz from water resonance in laboratory experiments, saturation effects have been observed that do not require the presence of macromolecules (1, 15, 16, 19–22). These effects are inversely proportional to the saturation pulse frequency offset and are considered contaminants in pure MT experiments. Thus, in this lower range of frequency offsets used in clinical imaging, mechanisms of saturation other than MT appear to be present.

Because of the clinical potential for off-resonance saturation imaging, it is important to understand the specific mechanisms involved for a given set of pulse parameters. The purpose of this investigation was to characterize tissue saturation on a clinical scanner, specifically in the lower range of frequency offsets, where non-MT effects have been observed. More important, our goal was to determine whether these near-resonance non-MT effects are useful clinically in evaluating pathologic conditions of the brain. We approached this problem by studying the effect of varying the frequency offset on T1-weighted images of a variety of phantom materials, as well as on T1-weighted, spin-density-weighted, and T2-weighted images of normal brain and pathologic lesions. By doing this we hoped to gain insight into underlying off-resonance saturation mechanisms and to optimize the technique for clinical neuroimaging.

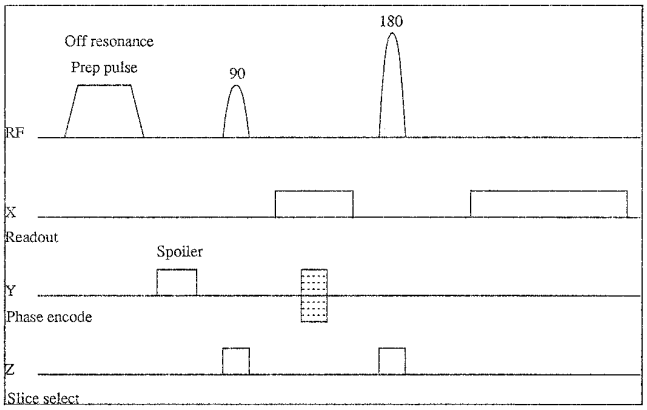

Fig 1. Diagram illustrates off-resonance saturation pulse applied before standard spin-echo imaging sequence is obtained. Pulse width is 16 milliseconds for T1-weighted images and 19.2 milliseconds for T2-weighted images; the bandwidth is 200 Hz for both sequences. *RF* indicates radio frequency.

Materials and Methods

Saturation Pulse

MR imaging was performed on a 1.5-T unit (Signa, General Electric Medical Systems, Milwaukee, Wis). The off-resonance saturation pulse used (Fig 1) had a bandwidth of 200 Hz. The pulse shape was an apodized sinc function with no side lobes and a duration of 16 milliseconds for T1-weighted sequences and 19.2 milliseconds for spin-density-weighted and T2-weighted sequences. The peak pulse amplitude was 9.5 μT for T1-weighted sequences and 14 μT for spin-density-weighted and T2-weighted sequences. After each saturation pulse, gradient homospoiling was performed by turning on the y-axis (phase-encoding) gradient to maximum amplitude for about 5 milliseconds. Allowing for gradient ramp times, the interval between the end of the saturation pulse and the beginning of the 90° pulse was approximately 6 milliseconds. The multisection off-resonance saturation pulses are nonselective and their saturation effects are cumulative throughout the repetition time.

Imaging Parameters

Axial T1-weighted images were acquired with and without the off-resonance saturation pulse with imaging parameters of 650/30/1 (repetition time [TR]/echo time [TE]/excitations), 24-cm field of view, 256 × 192 matrix, 5-mm section thickness, 2-mm intersection gap, and flow compensation. Imaging time for the T1-weighted spin-echo sequence (20 sections) with and without the off-resonance saturation pulse applied was 4 minutes, 34 seconds. The imaging parameters for conventional and off-resonance saturation spin-density-weighted and T2-weighted axial images were 3000/30,90/0.75, 24-cm field of view, 192 × 256 matrix, 5-mm section thickness, and 2-mm gap. The total imaging time for both conventional spin-echo and off-resonance saturation spin-density-

weighted and T2-weighted image acquisitions (18 sections) was 7 minutes, 48 seconds. Receive and transmit attenuator settings were held constant for comparable pulse sequences for each experiment.

Frequency Offset

Off-resonance saturation pulse T1-weighted imaging with frequency offsets of 50, 100, 150, 200, 300, 500, 1000, 2000, 5000, 10000, and 20 000 Hz down field from water resonance were used for human volunteers, and offsets of 100, 200, 300, 600, 1200, 2400, 5000, 10000, 15000, and 20 000 Hz were used for phantom experiments. For spin-density-weighted and T2-weighted images, the frequency offsets used were 100, 200, 300, 600, 1200, 2400, 7500, and 20 000 Hz down field from water resonance. Approval for the use of off-resonance saturation pulse imaging was obtained from our local institutional review board and from GE Medical Systems to operate the MR imager in an investigational mode. Specific absorption rates were carefully monitored in human studies and remained below limits mandated by the Food and Drug Administration (average, 3.2 W/kg for the whole head and 8.0 W/kg for any single gram of tissue).

In a separate experiment, the T2 weighting produced by the off-resonance saturation pulse was simulated on long TR images (with no pulse applied) by increasing the TE. With the TR constant at 3000, images with TEs of 75 and 135 and no saturation pulse were compared with images with TEs of 30 and 90 in which a saturation pulse was applied at a frequency offset of 300 Hz.

Phantom Experiments

Saturation pulse imaging on T1-weighted images was performed on phantom materials within plastic bottles at the frequency offsets described above. The materials included 4% agar, 2% agar, 1% agar, distilled water, 0.5 mM and 1 mM gadopentetate dimeglumine in solution, and 1 mM manganese chloride ($MnCl_2$) in solution. The T1 and T2 relaxation times for the phantom materials were calculated from a multiecho long-TR study using software provided on the GE Signa scanner.

Human Experiments

The imaging studies were explained to all subjects and informed consent was obtained. The off-resonance saturation sequences were tested in 10 healthy volunteers (5 men and 5 women, 26 to 49 years of age) who underwent noncontrast T1-weighted imaging, and in 10 healthy volunteers (5 men and 5 women, 22 to 47 years of age) who underwent spin-density-weighted and T2-weighted imaging. Off-resonance saturation imaging at 300 Hz offset was performed in 4 healthy volunteers (2 men and 2 women) with spin-density-weighted and T2-weighted sequences, and compared with nonsaturated sequences in which the TR was kept constant (3000) and the TE was lengthened as described above.

To determine whether near-resonance saturation pulses can improve lesion detection on T1-weighted sequences, several patients with pathologic conditions were scanned after administration of contrast material at offsets of 1200, 600, and 300 Hz from water resonance and compared with nonsaturated T1-weighted sequences. The pathologic conditions included meningeal neoplasm, venous angioma, metastases, primary neoplasm, and stroke. Improved visibility of enhancing lesions was judged subjectively by unanimous agreement of three neuroradiologists. To assess lesion contrast on T2-weighted and spin-density-weighted images, we also applied saturation pulse offsets of 1200, 600, and 300 Hz to long-TR sequences in several patients with abnormalities (stroke, neoplasm, gliosis).

Tissue Measurements

Quantitative signal analysis was performed in nine regions of interest: cerebrospinal fluid, frontal white matter, corpus callosum, putamen, thalamus, caudate, red nucleus, and substantia nigra (pars reticularis and pars compacta). These measurements were obtained with the use of conventional imager software by delineating a region of interest on the designated area in order to obtain a mean signal intensity measurement at each frequency offset. The size and location of the region of interest cursor were not changed between each set of acquisitions; visual assessment of the images confirmed that no significant patient motion or image misregistration had occurred. For all quantitative determinations, the median signal intensity of at least three independently obtained measurements was used. A region of interest was placed outside the cranium to obtain noise measurements, which were consistent across the range of frequency offsets studied in each patient.

Ratios

For each pulse sequence, suppression ratios were calculated with the formula $SR = (SI_o - SI_s)/SI_o$, where SR is the suppression ratio, SI_o is the signal intensity of the tissue or phantom material before the saturation pulse was applied, and SI_s is the signal intensity after the saturation pulse was applied. Calculation of the suppression ratio has been used by a number of investigators to quantify the extent of saturation of a given tissue using off-resonance pulse sequences. The SR indicates the proportion of signal loss that occurred during the saturation and $1-SR$ is the relative remaining signal. To quantify the effects of off-resonance saturation pulses on lesion conspicuity in some patients, contrast-to-noise ratios (CNR) were calculated by the formula $CNR = (S_a - S_b)/n$, where S_a is the signal intensity of the lesion of interest, S_b is the signal intensity of the background parenchyma, and n is the standard deviation of the noise.

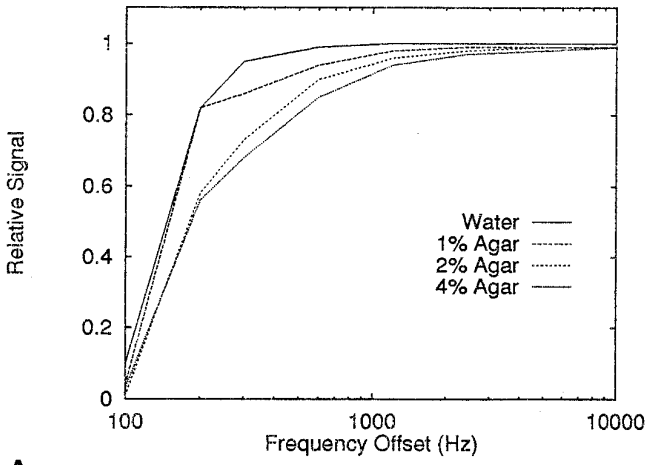

A

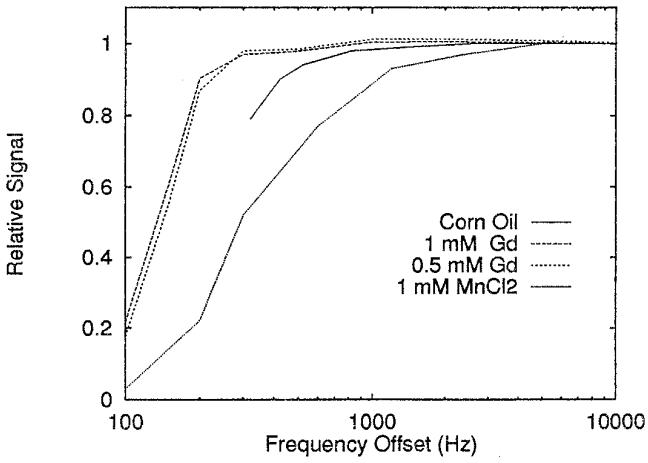

B

Fig 2. Graphs show relative signal at frequency offsets from 100 Hz to 10 000 Hz for phantom materials.

A, Direct suppression of distilled water occurs at approximately 300 Hz offset. Suppression of agar is inversely proportional to water content and, hence, T2 relaxation time.

B, Note that suppression of $MnCl_2$ solution is greater than other materials, occurring at offsets below 2000 Hz. Corn oil suppressed at offsets within 800 Hz of fat resonance (600 Hz from water resonance), whereas contrast material was relatively unaffected by the off-resonance pulse above 300 Hz.

Results

Phantom Experiments

Figure 2 shows the effect of off-resonance saturation pulses on T1-weighted images of agar, 1 mM $MnCl_2$, 0.5 mM and 1 mM gadopentetate dimeglumine, corn oil, and distilled water. Suppression of agar concentrations increased as the frequency offset was decreased toward water resonance (Fig 2A). The degree of suppression was inversely proportional to the free water content with distilled water suppressing the least and 4% agar suppressing the most.

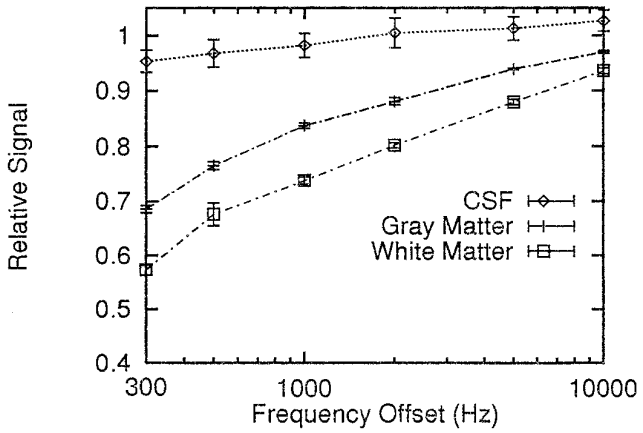

Fig 3. Graph shows relative signal (error bars represent ± 1 SD) of representative normal brain tissues (caudate, white matter, cerebrospinal fluid [*CSF*]) from 10 volunteers on T1-weighted images with saturation pulses at frequency offsets from 300 Hz to 10 000 Hz. Note progressively greater suppression of white matter relative to gray matter as the frequency offset is reduced. CSF shows least suppression across the range of offsets studied.

On the T1-weighted images, this differential suppression increased the contrast between the agar concentrations as the frequency offset was decreased to approximately 300 Hz. Direct saturation of distilled water did not occur until the frequency offset was brought within a range of 200 Hz to 300 Hz down field from water resonance (Fig 2A).

T1-weighted off-resonance saturation images of a 1-mM solution of $MnCl_2$ showed dramatic suppression at frequency offsets below 2000 Hz from water resonance, despite the fact that no macromolecules were present in the solution (Fig 2B). Likewise, corn oil suppressed at frequency offsets within 800 Hz from fat resonance (600 Hz from water resonance) (Fig 2B). Suppression of $MnCl_2$ was greater than that of any of the other phantom materials investigated and greater than that of brain tissue at 300 Hz frequency offset (Fig 3). This is very different from the contrast solutions, which showed no significant suppression until frequency offsets below 300 Hz were reached (Fig 2B). On T1-weighted images, saturation of phantom solutions containing no macromolecules (hence no MT effect) was present only in those materials with a relatively short T1 relaxation time and a large T1/T2 ratio ($MnCl_2$ and corn oil), whereas those with a long T1 relaxation time (water) or those with a T1/T2 ratio near unity (gadopentetate dimeglumine) were unaffected except at very low offsets (<300 Hz) (see Table).

Suppression versus T1/T2 ratios for phantom materials

Material	T1/T2 (Ratio)	Suppression (300 Hz), %
0.5 mM gadopentetate dimeglumine	393 /343 (1.2)	3
1.0 mM gadopentetate dimeglumine	214 /178 (1.2)	3
Water	2873/1400 (2.1)	5
Corn oil	240 /48 (5.0)	21*
1.0 mM $MnCl_2$	144 /14 (10.3)	48

Note.—Phantom materials: Relative T1 and T2 relaxation times and suppression at a frequency offset of 300 Hz for simple solutions containing no macromolecules of gadopentetate dimeglumine, $MnCl_2$, water, and corn oil. Note that substances with a T1/T2 much greater than 1.0 (similar to ratios seen in tissues) are suppressible, while those closer to unity and those with a very long T1 are relatively unaffected. Values calculated by least squares fit from data acquired at 1.5 T using six-point inversion recovery and multiple TE spin-echo sequences.

* 100 Hz from water resonance, 320 Hz from fat resonance.

Normal Brain Tissues: T2-Sensitive Saturation on T1-Weighted Images

As expected from the phantom experiments, suppression of normal intracranial structures (except cerebrospinal fluid) on T1-weighted images dramatically increased as the saturation pulse frequency offset was decreased (Fig 3). At frequency offsets below 300 Hz, direct water suppression and susceptibility artifacts from the skull base limited adequate visualization of normal structures. An offset of 300 Hz was subjectively judged by 3 neuroradiologists to be optimal for maximal suppression while maintaining adequate visualization of normal structures in each of the 10 volunteers.

Suppression of normal brain on T1-weighted images resulted in altered contrast between the specific brain structures (Fig 4). No tissue suppression was seen at 20 000 Hz frequency offset. As the frequency offset was brought closer to water resonance, there was progressively greater suppression of white matter structures relative to deep and cortical gray matter structures (Figs 3 and 4). The overall effect of this

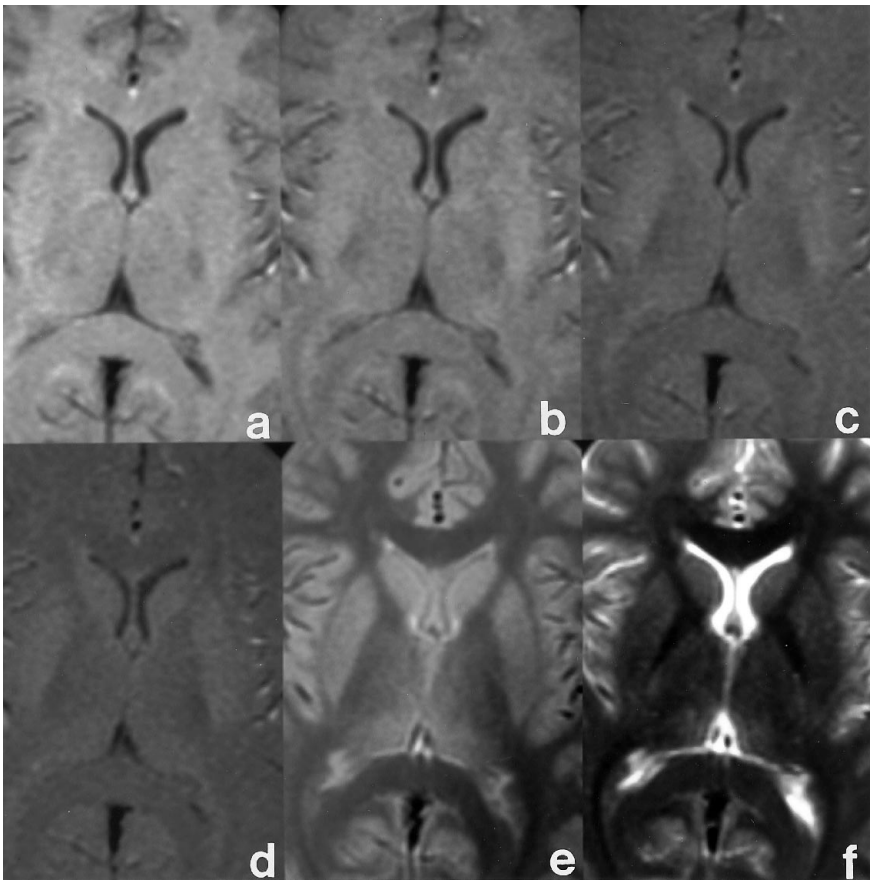

Fig 4. MR images of the brain at the level of the basal ganglia. T1-weighted spin-echo images with an off-resonance saturation pulse applied at 20 000 Hz (*a*), 2000 Hz (*b*), 500 Hz (*c*), and 300 Hz (*d*) frequency offset, compared with long-TR (3000) images at TEs of 30 (*e*) and 90 (*f*). Note on *a* through *d* that differential tissue suppression results in progressive T2-weighted tissue contrast of the deep and cortical gray matter structures relative to adjacent white matter structures, giving an appearance similar to the long-TR sequences. All window settings are constant for T1-weighted sequences.

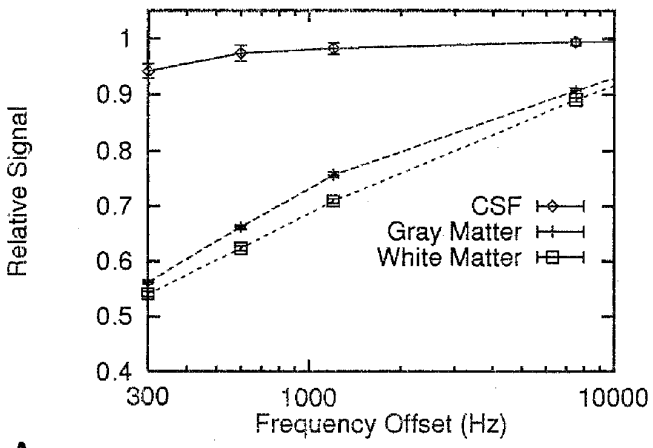

A

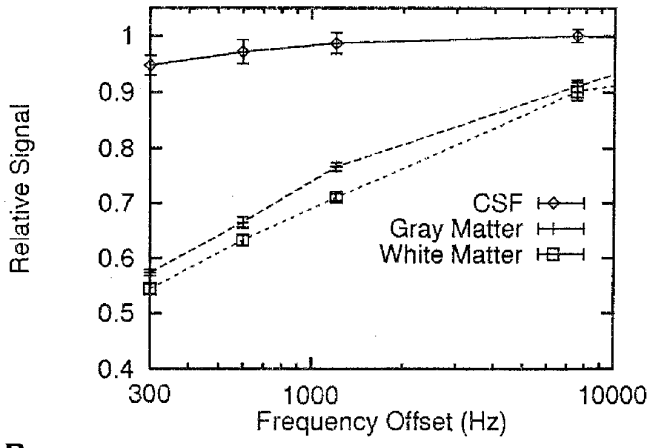

B

Fig 5. Graphs show relative signal (error bars represent ± 1 SD) of representative normal tissues (caudate, white matter, CSF) of 10 volunteers on spin-density-weighted images (3000/30) (*A*) and T2-weighted images (3000/90) (*B*) at saturation pulse frequency offsets ranging from 300 Hz to 10 000 Hz. There is little suppression of CSF as compared with brain tissue.

process on the appearance of the intracranial structures was to increase T2 effects on T1-weighted images, such that tissue contrast was similar to that seen on T2-weighted images (Fig 4). As expected from the corn oil phantom, extracranial fatty tissues showed little suppression at frequency offsets above 300 Hz from water resonance but demonstrated approximately 15% suppression at 100 Hz offset (320 Hz from fat resonance).

Normal Brain Tissues: T2-Sensitive Saturation on Spin-Density-Weighted and T2-Weighted Images

Off-resonance saturation pulses applied to spin-density-weighted and T2-weighted images of healthy volunteers resulted in dramatically increased suppression as the frequency offset was brought closer to water resonance (Fig 5). As was the case with the T1-weighted images, loss of anatomic detail from direct water saturation and susceptibility artifacts from the skull base limited visualization of normal structures at frequency offsets below 300 Hz. As the frequency offset was decreased and suppression was increased, spin-density-weighted images began to show tissue contrast characteristics similar to standard T2-weighted images (Fig 6A–C). Likewise, when a saturation pulse was applied to T2-weighted pulse sequences, images appeared progressively more T2-weighted as the frequency offset was reduced (Fig 6D–F).

Increasing the TE: Simulation of a T2-Sensitive Saturation Mechanism

Reducing the frequency offset of the saturation pulse applied to spin-density-weighted images produced increased T2-weighted contrast (Fig 6); an effect similar to increasing the TE of long TR pulse sequences. Figure 7A shows that with a constant, long TR (3000), increasing the TE can yield similar suppression and contrast between gray matter, white matter, and cerebrospinal fluid as did the near-resonance saturation pulse technique. However, there are subtle differences in image contrast particularly in iron-containing structures (Fig 7B) when these two techniques are compared, suggesting that saturation mechanisms in some tissues are not simply equivalent to T2-weighting.

Lesions: T1-Weighted, Spin-Density-Weighted, and T2-Weighted Images

As seen in normal brain tissues, off-resonance saturation pulses applied to T1-weighted images in patients with pathologic conditions resulted in tissue contrast similar to that seen on T2-weighted images (Fig 8). In other words, there was a relative lack of suppression of tissues known to have long T2 relaxation times. This was demonstrated in patients with a number of pathologic conditions, including metastases, primary neoplasm with vasogenic edema, acute stroke, and demyelination. The end result was that lesions, poorly delineated on T1-weighted images and hyperintense on T2-weighted images, had slightly increased signal on near-resonance saturated T1-weighted im-

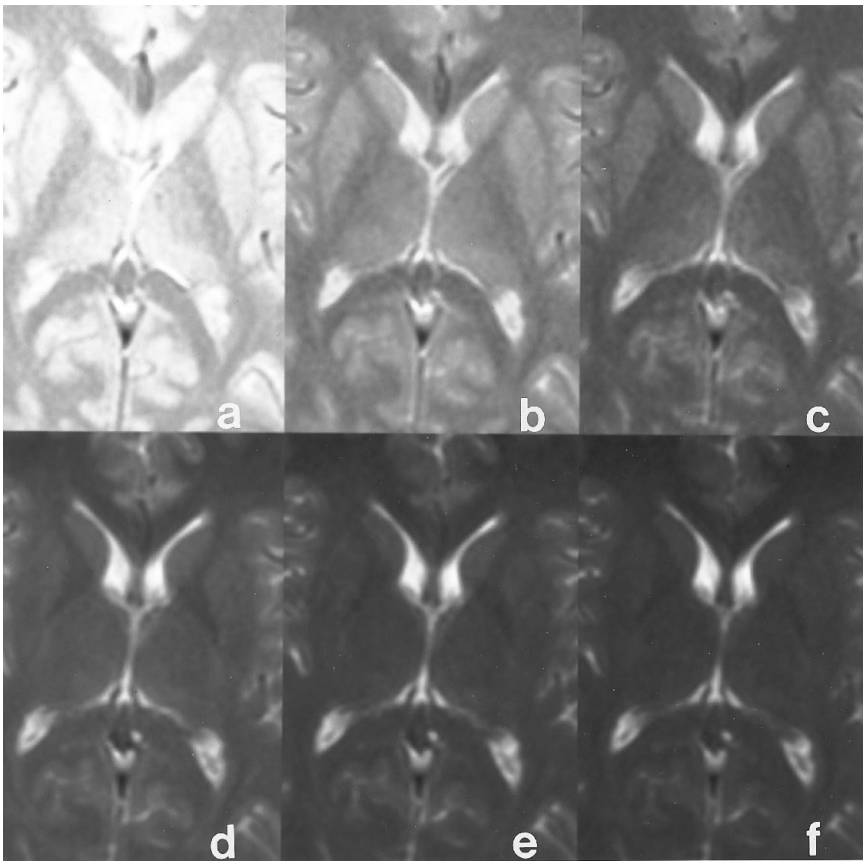

Fig 6. MR images of the brain at the level of the basal ganglia. Spin-density-weighted images (3000/30) (*top row*) and T2-weighted images (3000/90) (*bottom row*) obtained after an off-resonance saturation pulse applied at 20 000 Hz (*a* and *d*), 1200 Hz (*b* and *e*), and 300 Hz (*c* and *f*) frequency offset from water resonance. On both the spin-density-weighted and the T2-weighted images there is progressive suppression and T2 contrast of tissues as the frequency offset is reduced. Note the progressive loss of gray–white differentiation, presumably related to T2 weighting from the off-resonance saturation pulse. All window settings are constant.

ages relative to adjacent brain structures. Near-resonance saturation of spin-density-weighted and T2-weighted sequences resulted in similar differential suppression of tissues with different T2 relaxation times. However, increased lesion conspicuity was seen most often on the spin-density-weighted images and was generally not present on T2-weighted images; this effect is most likely related to the specific T2 relaxation times of the various pathologic disorders studied (gliosis, stroke, neoplasm), specific sequence timing parameters, and reduced signal-to-noise ratios on the saturated images (Fig 9).

As might be expected from the relative lack of suppression of contrast solution (Fig 2B), an off-resonance saturation pulse applied to T1-weighted sequences with enhancing lesions resulted in increased lesion conspicuity in most cases as the frequency offset was decreased (Fig 10). This effect results from the differential suppression between contrast material and normal brain structures and was seen in patients with a variety of pathologic conditions, including meningeal neoplasm, venous angioma, metastases, primary neoplasm, and stroke.

Discussion

Recently, there has been considerable interest in applying off-resonance radiation to routine MR imaging sequences in order to alter image contrast. To accomplish this, a preparatory pulse of low amplitude and short duration is applied at a specific frequency offset down field from water resonance before a conventional imaging sequence is performed. Although standard off-resonance pulse sequences are now available commercially, the optimal pulse parameters for given pathologic conditions have not been fully explored. Tissue contrast observed empirically with these methods has been attributed to MT, a phenomenon by which MR signal from free protons is modulated by selective saturation of restricted protons associated with macromolecules (1, 14–16). However, there are "direct" saturation effects that occur in the lower range of frequency offsets currently used clinically (<2000 Hz) and that clearly do not depend on the macromolecular pool (1, 15, 16, 19–22). Although these effects are considered contaminants in pure laboratory MT exper-

Fig 7. Increasing the TE on long-TR (3000) sequences simulates near-resonance saturation effect on images at the level of the basal ganglia.

A, *Top row:* Spin-density-weighted image (3000/30) (*a*), spin-density-weighted image (3000/30) with near-resonance saturation pulse (300 Hz) (*b*), and long-TR image (3000/75) without saturation pulse applied (*c*).

Bottom row: T2-weighted image (3000/90) (*d*), T2-weighted image with near-resonance saturation pulse (300 Hz) (*e*), and long-TR image (3000/135) without saturation pulse applied (*f*). Near-resonance saturation pulse applied to spin-density-weighted and T2-weighted images at 300 Hz frequency offset results in tissue suppression and tissue contrast characteristics simulated by lengthening the TE to 75 and 135, respectively, in the absence of off-resonance radiation. All window settings are constant.

B, *Top row:* Spin-density-weighted image (3000/30) (*g*), spin-density-weighted image (3000/30) with near-resonance saturation pulse (300 Hz) (*h*), and long-TR image (3000/75) without saturation pulse applied (*i*). *Bottom row:* T2-weighted image (3000/90) (*j*), T2-weighted image (3000/90) with near-resonance saturation pulse (300 Hz) (*k*), and long-TR image (3000/135) without saturation pulse applied (*l*). There are subtle differences in tissue contrast characteristics within iron-containing structures between these sequences. Note that the globus pallidus shows less signal on the image obtained without the saturation pulse but with a TE of 75 (*i*) compared with routine spin-density-weighted image (TE, 30) after near-resonance pulse has been applied (*h*). All window settings are constant.

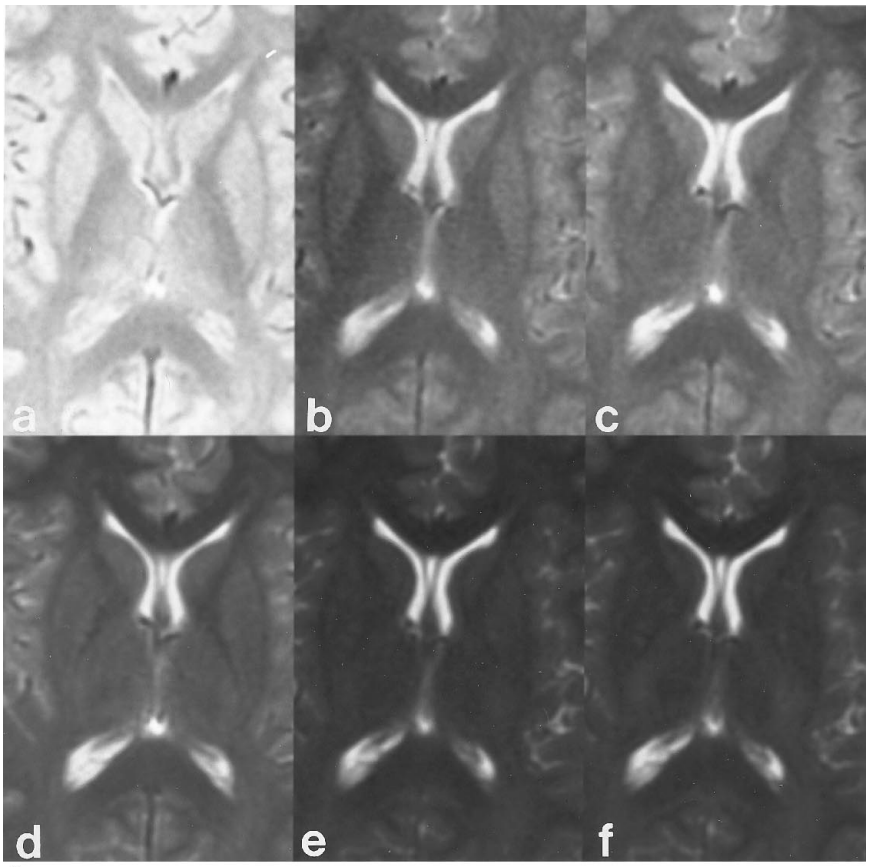

A

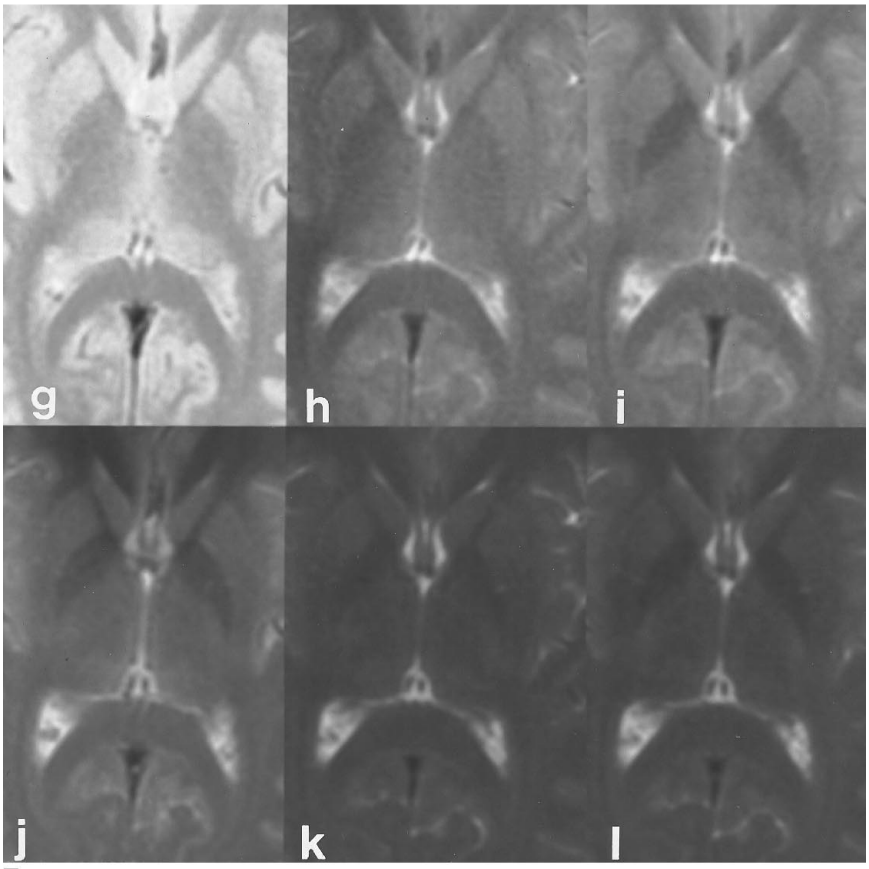

B

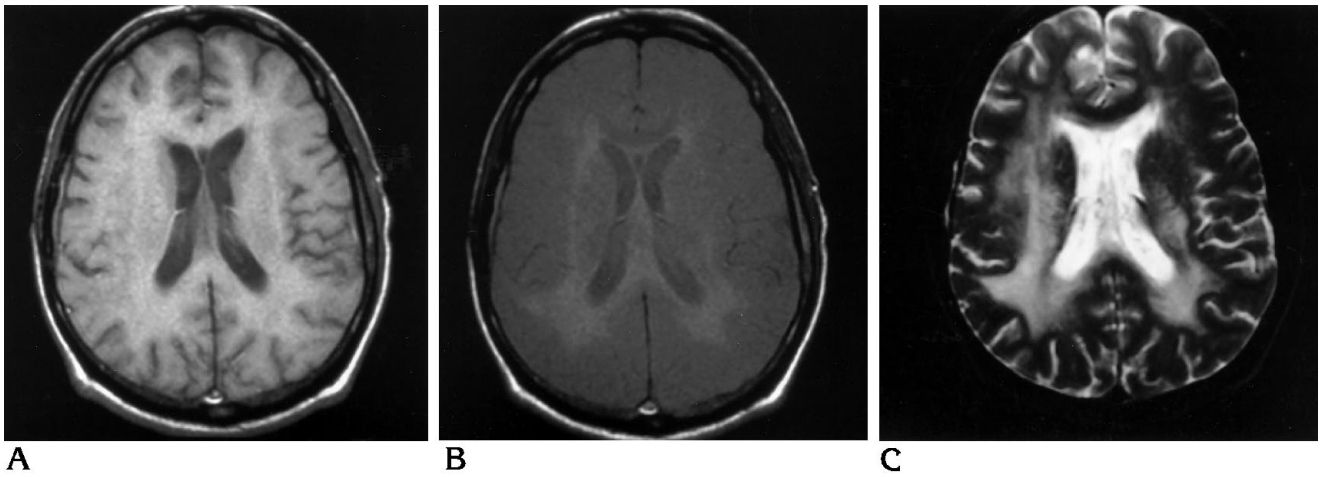

Fig 8. A 56-year-old man with diffuse radiation changes of the cerebral white matter and corpus callosum.

A, T1-weighted image. Note that when a near-resonance saturation pulse is applied at 300 Hz (*B*), there is a relative lack of suppression of the diseased white matter and corpus callosum compared with normal brain tissue. The net result is increased signal of the diseased tissue relative to normal brain, giving T2 tissue characteristics similar to that seen on the T2-weighted image (*C*). Window settings are constant for T1-weighted images.

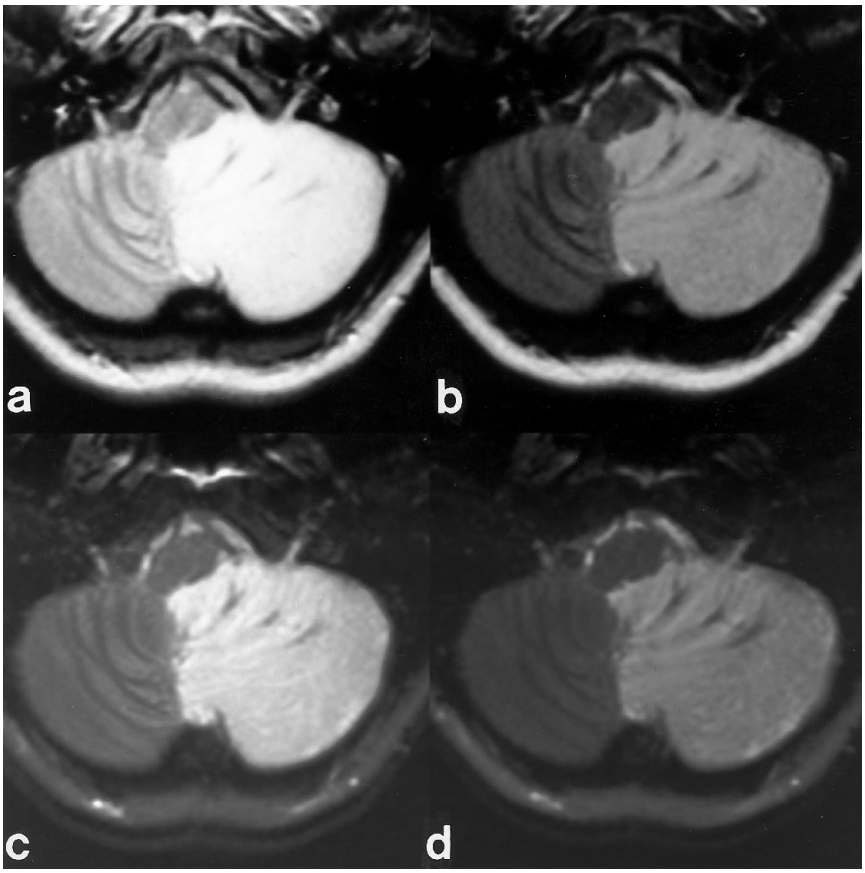

Fig 9. A 35-year-old woman with an acute cerebellar infarct.

Spin-density-weighted images (*a* and *b*) and T2-weighted images (*c* and *d*). Increased visual conspicuity between the infarct and normal brain on spin-density-weighted image after application of saturation pulse at 300 Hz offset (*b*) coincides with an increase in the contrast/noise ratio from 22.8 to 26.0. This effect is not evident on the T2-weighted sequence after application of saturation pulse at 300 Hz (*d*), since a loss of signal-to-noise ratio results in a decreased contrast/noise ratio from 74.0 to 68.9. All window settings are constant.

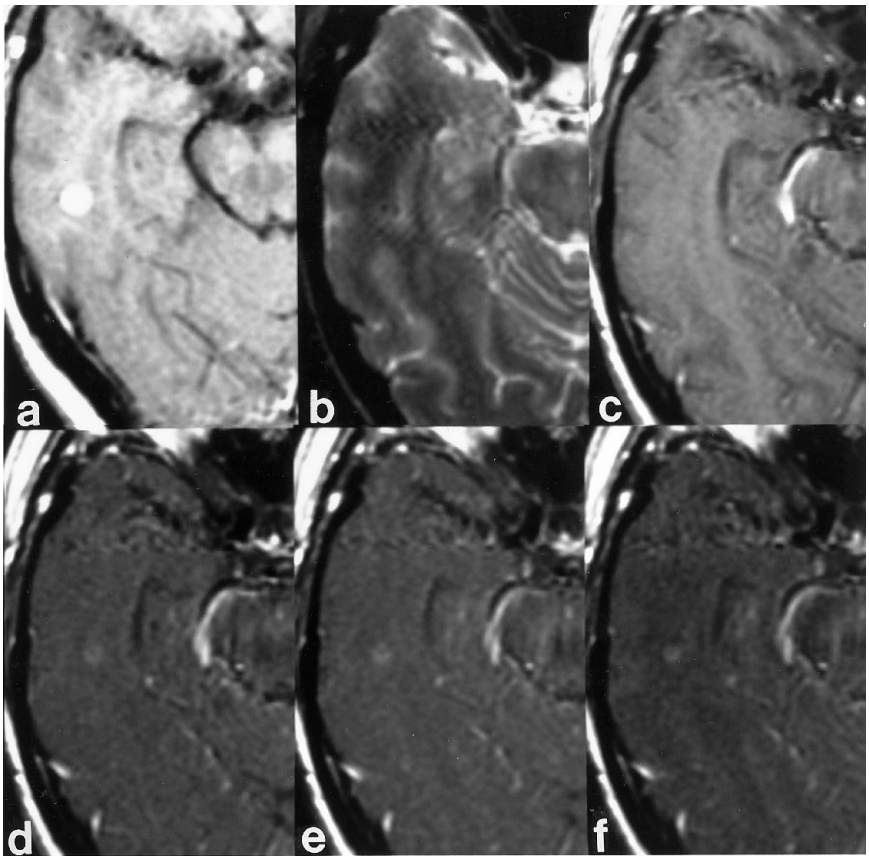

Fig 10. A 63-year-old man with metastatic melanoma.

T1-weighted image (*a*) shows metastatic lesion before chemotherapy. T2-weighted (*b*) and contrast-enhanced T1-weighted (*c*) images obtained 8 months after treatment show no detectable lesion. When an off-resonance saturation pulse is applied to a postcontrast T1-weighted sequence at frequency offsets of 1200 Hz (*d*), 600 Hz (*e*), and 300 Hz (*f*), a residual right temporal lobe lesion becomes visible. Maximum contrast between the enhancing lesion and normal brain is at frequency offset of 300 Hz (*f*) down field from water. Window settings are constant for *c* through *f*.

iments, our $MnCl_2$ results suggest that they also contribute to tissue contrast with pulse parameters currently used in practice on clinical scanners. Furthermore, these same non-MT effects have the potential to improve detection of pathologic lesions within the central nervous system significantly.

To understand fully the importance of the observations regarding $MnCl_2$, one should consider the relaxation properties of aqueous solutions containing paramagnetic ions that are explainable in terms of the theory developed by Solomon (23) and later modified by Bloembergen and Morgan (24). Such analysis shows that change in solution relaxation rates (1/T1 and 1/T2) due to a paramagnetic ion (such as gadolinium) is proportional to the concentration of that ion and its specific relaxivity ($X1_{Gd}$ or $X2_{Gd}$). For Gd^{+3} (and most other metallic aquoions), X1 and X2 are approximately equal. Consequently, the ratio T1/T2 is approximately unity for aqueous solutions of most paramagnetic agents in low concentrations (25). The aqueous Mn^{+2} ion, on the other hand, has long been known to have aberrant relaxation behavior, particularly in the 10 MHz to 100 MHz range (26, 27). For Mn^{+2}, the ratio X2/X1 is significantly greater than unity, ranging from 2.6 (at 6 MHz) to 7.5 (at 50 MHz). The physical basis of this behavior is complex, but relates to the fact that in this range of MR imaging frequencies, a powerful spin-exchange interaction exists between electron spins in Mn^{+2} and nuclear spins in water protons in the first coordination sphere (25).

At 64 MHz, the disparate T1/T2 behavior between simple solutions of $MnCl_2$ and gadopentetate dimeglumine becomes apparent (see Table). In low concentrations, contrast solutions exhibit T1/T2 values close to unity, similar to ratios of pure liquids. Because of short T2 relaxation times, $MnCl_2$ solutions have T1/T2 much greater than 1.0, similar to values recorded for solid tissues, such as brain. The behavior of $MnCl_2$ in our saturation experiments cannot be due to MT interactions with macromolecules, because no macromolecules are present. The saturation effects we see at low frequency offsets must therefore have another explanation, presumably based on relative differences in the T1 and T2 relaxation times of the various substances (20) (see Table). A recent

investigation into the behavior of these simple solutions in the presence of near-resonance irradiation found that magnetic relaxation could be described by using Bloch's equations transformed to an alternative, spin-lock coordinate system (28) (see Appendix).

In spin-lock imaging, tissue contrast is altered by exploiting an effective relaxation time known as $T1_\rho$, in a rotating frame of reference (21, 29–31). Traditional methods have used high-amplitude continuous wave radio frequency pulses that are limited by specific absorption rate considerations in higher field strength units. More recently, off-resonance spin-lock imaging techniques have been developed that use pulses of low amplitude that can affect tissue contrast in high-field systems without losing the benefits of an adequate signal-to-noise ratio (21, 30, 31). The degree of saturation achieved with these techniques in phantom materials, such as agar, is highly sensitive to the frequency offset of the radio frequency pulse. With frequency offsets far removed from water resonance, $T1_\rho$ will approach T1 relaxation time. However, as the frequency offset is brought closer to water resonance, the magnetization relaxes more rapidly toward a new, smaller equilibrium, M_ρ(EQ). This new equilibrium can range from 100% of the M_o when no spin-lock effect is present (offset far removed from water resonance) to 0% of M_o when the saturation pulse is on resonance. Several investigators have used spin-lock techniques to suppress tissues selectively and improve contrast between normal structures and abnormal lesions, including in vitro and in vivo breast lesions (30, 31) and tumors in mice that contain paramagnetic substances (32). However, the spin-lock sequences used for these applications are not practical for clinical neuroimaging.

Clearly, research is necessary to determine the potential interplay between MT and spin-locking at the lower range of frequency offsets used in clinical imaging, and to determine specific macromolecule binding characteristics that may account for each phenomenon. However, our $MnCl_2$ results do suggest that non-MT effects, presumably spin-lock excitation, account for a significant proportion of the saturation observed in clinical imaging at frequency offsets below 2000 Hz from water resonance. In our experiments, suppression of normal white matter was dramatically increased from approximately 20% to approximately 45% as the off-resonance pulse was decreased from 2000 Hz to 300 Hz. Offsets below 300 Hz resulted in saturation of free water protons, most likely due to spin-tip effects (28) and, consequently, caused marked reduction of image quality. Note, however, that the magnitude of a spin-lock effect and the specific frequency offset at which it begins to contribute to image contrast depend on pulse amplitude and design. The larger the pulse amplitude, the farther away from water resonance spin-locking will occur. In addition, the pulse design must be adiabatic in nature with a gradual rise/fall time in order to achieve spin-locking and to avoid direct spin-tip effects.

Analysis of simple solutions suggests that signal saturation due to near-resonance spin-locking is greatest in materials with a short T1 relaxation time and a relatively large T1/T2 ratio (28). Our in vitro and in vivo data support the idea that a relatively large T1/T2 ratio is necessary for semisolid and liquid materials (agar, $MnCl_2$, corn oil) and tissue (brain, fat) to be susceptible to spin-lock excitation, whereas those substances with T1/T2 ratios closer to unity (contrast material) or those with very long T1 relaxation times (cerebrospinal fluid, water) are relatively unaffected (see Appendix). Likewise, pathologic lesions showing a proportionally greater increase in T2 compared with T1 relative to normal brain (ie, tumor, edema, demyelination) should be less saturated, causing relative T2 weighting of T1-weighted images. This was a consistent finding in our study, wherein lesions that were poorly seen on T1-weighted images but hyperintense on T2-weighted images showed relative T2 contrast when near-resonance radiation was applied.

To appreciate the effects of spin-lock excitation and MT on tissue contrast, one must have an understanding of mechanisms at the molecular level responsible for T1 and T2 relaxation times. Specifically, the T1 and T2 of a particular tissue is dependent on the interaction of water with hydrophilic macromolecules in that tissue (1, 33, 34). The extremely short T2 of these macromolecules (ie, microseconds) does not allow them to be visible on routine clinical images. Nevertheless, they exert an effect on tissue contrast by restricting proton movement and decreasing relaxation times (T2 proportionally more than T1) of the visible water molecules. Consequently, these interactions are responsible for both the transfer of energy from

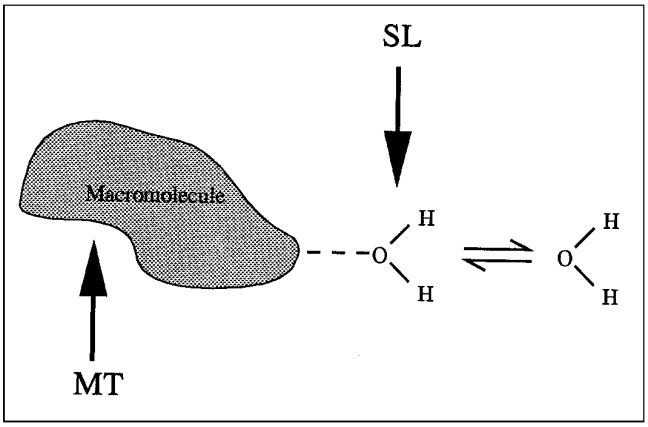

Fig 11. Simplified model of the effects of tissue macromolecules in the presence of near-resonance radiation, showing that water molecules in the hydration layer of macromolecules are susceptible to both MT and spin-lock (*SL*) excitation.

macromolecule to water molecule in MT and for shortening T2 relative to T1, causing tissues to be susceptible to spin-lock (21, 28, 31, 34). While macromolecules clearly influence the spin-lock effect in tissues, the presence of macromolecules is not obligatory for it to occur (28). In other words, water molecules in the hydration layer of macromolecules are susceptible to both spin-locking and MT (Fig 11), but these phenomena act by distinctly different mechanisms and at different frequency offsets. One can expect both mechanisms to affect susceptible tissues maximally with a relatively short T2 relaxation time (and long correlation time) arising from macromolecule-water interactions, thereby producing qualitatively T2-weighted contrast (14, 21, 30, 31, 35–38).

The tissue contrast observed in our investigation has significant clinical import in the evaluation of pathologic lesions within the brain. On off-resonance saturated T1-weighted images, parenchymal lesions with long T2 relaxation times (ie, edema, tumor, demyelination, stroke) will be slightly hyperintense relative to adjacent brain, and if contrast material has been administered, this hyperintense signal could be confused with subtle enhancement when in fact no enhancement is present. Additionally, one can expect to see greater suppression of normal tissue relative to adjacent lesions with long T2 relaxation times on spin-density-weighted and T2-weighted images. Conspicuity of brain structures and lesions on these long-TR sequences, however, depends on the specific T2 of the tissue being imaged and on the relative loss of signal-to-noise ratio from the saturation pulse. In essence, for brain tissue, the net qualitative effect of introducing spin-locking by decreasing the saturation pulse frequency offset toward water resonance is to add T2 weighting to whichever sequence is being used. However, further research is necessary to determine how spin-lock contrast may differ quantitatively from T2-weighted contrast at field strengths used in clinical neuroimaging.

One of the most interesting and useful findings of our investigation is the differential suppression of contrast material relative to normal brain structures as the off-resonance saturation pulse is brought closer to water resonance. With this in mind, one can expect a significant improvement in the visibility of enhancing lesions relative to normal adjacent brain as the frequency offset is decreased to approximately 300 Hz. Clearly, more research is needed to determine the optimal parameters for detecting subtle enhancing lesions within the brain. However, our experiments in evaluating gadopentetate dimeglumine in solution and our observations of several patients with enhancing brain lesions do suggest that use of near-resonance spin-lock contrast can significantly improve lesion detection over standard T1-weighted images and also over commercially available MT saturation sequences that use larger frequency offsets.

Summary

Near-resonance saturation pulses most likely produce both spin-lock excitation and MT effects at the frequency offsets currently used in clinical imaging. Our data regarding offsets between 300 Hz and 2000 Hz are better explained by spin-locking as a determinant of image contrast than by MT alone. In this lower range of frequency offsets, only tissues with a short or intermediate T1 and a relatively large T1/T2 ratio are susceptible to spin-locking. Above this range, MT effects are probably more important than spin-locking effects in generating image contrast. Precise contributions or possible interactions of these two distinct mechanisms for a given set of pulse parameters are unknown and have yet to be examined on clinical scanners. Below 300 Hz, direct spin-tip excitation causes significant deterioration of image quality, negating the effects of spin-lock and MT.

By appreciating the spin-lock contribution to off-resonance saturation imaging, it is possible

to predict, in qualitative terms, what effect the technique will have on tissue appearance, which has important diagnostic implications. One can expect that a near-resonance saturation pulse applied to a T1-weighted sequence will add T2 weighting to the image and result in tissue contrast similar to that seen on a spin-density-weighted or T2-weighted image. Likewise, near-resonance radiation applied to a spin-density-weighted image will produce tissue contrast similar to that of a T2-weighted image. In addition, the differential suppression of contrast material relative to the brain parenchyma achieved by near-resonance spin-locking should yield considerably improved detection of enhancing lesions compared with standard T1-weighted images and commercially available MT sequences. With the pulse parameters used in this study, a frequency offset of 300 Hz down field from water resonance is optimal to achieve maximal differential suppression between brain and enhancing lesions, without significant loss of anatomic detail. However, when near-resonance saturation is used on T1-weighted images, the resulting hyperintensity of lesions with long T2 relaxation times could be mistaken for subtle enhancement if the postcontrast images are not compared with the precontrast images.

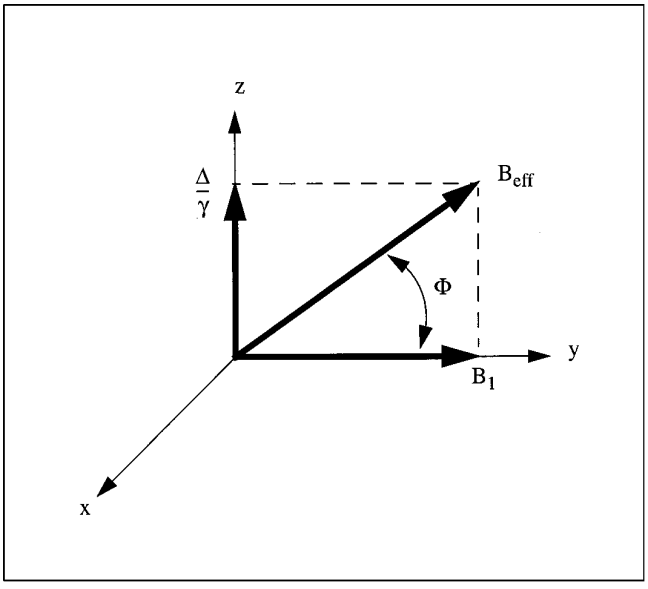

Fig A1. The effective fields in the rotating frame for off-resonance B_1.

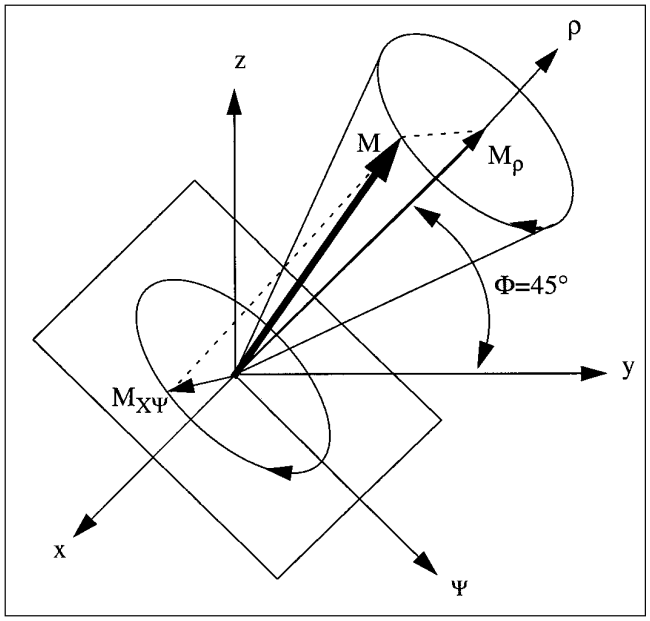

Fig A2. Spin-lock (M_ρ) and spin-tip ($MX\psi$) components of M for off-resonance excitation at 45°.

Appendix

In an MR imaging experiment, a radio frequency (RF) field, B_1, oscillating at a frequency ω_{RF}, is applied perpendicularly to the main magnetic field, B_0, which is oriented in the z direction. In the laboratory frame of reference, the RF field rotates about the B_0 field at rate ω_{RF}. Analysis is greatly simplified by viewing the experiment in a frame of reference rotating at the same rate as the RF field. Such a transformation to rotating-frame coordinates is equivalent to subtracting ω_{RF} from the Larmor frequency, $\omega_0 = \gamma B_0$, resulting in a z-directed field of $\Delta/\gamma = (\omega_0 - \omega_{RF})/\gamma$. The net effective field, B_{eff}, is then the vector sum of Δ/γ and B_1 oriented at an angle of $\Phi = \arctan[(\Delta/\gamma)/B_1]$. Figure A1 illustrates the rotating frame fields.

In the usual MR imaging experiment, Δ is zero; that is, the RF field is tuned to exactly match the Larmor frequency. The net effective field, about which the magnetization precesses perpendicularly, is simply B_1. Selection of a given B_1 amplitude and duration generates a desired flip angle as pure spin-tip in the x-z plane. The flip angle determines the amount of magnetization left in the x-y plane that then undergoes ordinary T1 and T2 relaxation until imaged.

In this study, we applied off-resonance excitation, where Δ is nonzero. If B_1 is off-resonance and is turned on slowly relative to the Larmor frequency—that is, $d\Phi/dt << \omega_0$—then the magnetization remains locked along the direction of B_{eff}. Such a mode of excitation is referred to as *spin-lock excitation*. Typically, an admixture of spin-tip and spin-lock excitation results, which precesses about B_{eff} in a cone. Figure A2 illustrates the resultant magnetization components for a spin-lock angle of 45°, where $B_1 = \Delta/\gamma$. (A B_1 of 10 μT corresponds to a Δ of 425 Hz.)

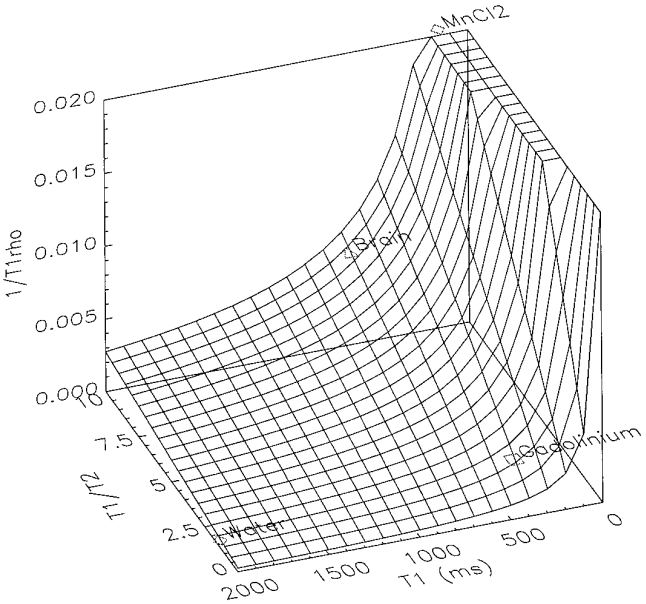

Fig A3. The degree of signal suppression in off-resonance spin-lock imaging is proportional to $1/T1_\rho$. T1 and T2 for four different materials are used to calculate $1/T1_\rho$ for an off-resonance angle of 45°. The materials are water (T1 > 2000; T2, 1400), 0.5 mM gadopentetate dimeglumine (393/343, T1/T2), white matter (700/74), and 1 mM $MnCl_2$ (144/14).

In a process analogous to ordinary T1 and T2 relaxation, $M\rho$ will tend to relax toward an equilibrium value, denoted $M_\rho(EQ)$, with time constant $T1_\rho$, and $Mx\Psi$ will decay toward zero with time constant $T2_\rho$. If spin-tip is avoided by appropriately shaping B_1 to limit $d\Phi/dt$, Bloch's equations reduce to a single simple spin-lock equation

A1) $$\frac{d}{dt} M_\rho(t) = -\frac{1}{T1_\rho}[M_\rho(t) - M_\rho(EQ)]$$

where

A2) $$\frac{1}{T1_\rho} = \frac{1}{T1}\sin^2\Phi + \frac{1}{T2}\cos^2\Phi$$

$$= \frac{1}{T1}(\sin^2\Phi + \frac{T1}{T2}\cos^2\Phi)$$

and

A3) $$M_\rho(EQ) = \frac{T1_\rho}{T1} M_0 \sin\Phi.$$

As Δ is lowered, Equation A2 shows that $T1_\rho$ will approach T2, since Φ is decreasing. Also note from Equation A3 that $M_\rho(EQ)$ is lowest for large values of $T1/T1_\rho$ and decreases as Δ is decreased. Near-resonance spin-lock contrast will therefore appear somewhat T2 weighted with greater suppression for materials with large T1/T2 ratios.

At the end of the pulse, M_{rho} will return to *z*-axis alignment, with its magnitude determined by the amount of $T1_\rho$ relaxation during the pulse as determined by T1, T2, and Δ. It is this magnetization that is then imaged with a standard spin-echo or gradient-echo pulse sequence. Any residual M_{xy} magnetization left in the x-y plane after the off-resonance pulse is typically spoiled by a large x or y gradient immediately after the pulse.

A plot of $1/T1_\rho$ for various T1 and T2 provides a useful qualitative understanding of spin-lock contrast. Figure A3 presents such a plot for T1 of 0 to 2000 milliseconds and a T1/T2 ratio of 0 to 10.

References

1. Wolff SD, Balaban RS. Magnetization transfer imaging: practical aspects and clinical applications. *Radiology* 1994; 192:593–599
2. Edelman RR, Ahn SS, Chien D, et al. Improved time-of-flight MR angiography of the brain with magnetization transfer contrast. *Radiology* 1992;184:395–399
3. Lin W, Tkach JA, Haacke EM, Masaryk TJ. Intracranial MR angiography: application of magnetization transfer contrast and fat saturation to short gradient echo, velocity-compensated sequences. *Radiology* 1993;186:753–761
4. Ordidge RJ, Helpern JA, Knight RA, et al. Investigation of cerebral ischemia using magnetization transfer contrast (MTC) MR imaging. *Magn Reson Imaging* 1991;9:895–902
5. Mathews VP, King JC, Elster AD, Hamilton CA. Cerebral infarction: effects of dose and magnetization transfer saturation at gadolinium-enhanced MR imaging. *Radiology* 1994;190:547–552
6. Finelli DA, Hurst GC, Gullapali RP, Bellon EM. Improved contrast of enhancing brain lesions on post gadolinium, T1-weighted spin echo images with use of magnetization transfer. *Radiology* 1994; 190:553–559
7. Elster AD, Mathews VP, King JC, Hamilton C. Improved detection of gadolinium enhancement using magnetization transfer imaging. *Neuroimaging Clin N Am* 1994;4:185–192
8. Ceckler TL, Karino K, Kador PF, Balaban RS. Magnetic resonance imaging of the rabbit eye: improved anatomical detail using magnetization transfer contrast. *Invest Ophthalmol Vis Sci* 1991;32: 3109–3113
9. Dousset V, Grossman RJ, Ramer KN, et al. Experimental allergic encephalomyelitis and multiple sclerosis: lesion characterization with magnetization transfer imaging. *Radiology* 1992;182:483–491
10. Lexa FL, Galetta SL, Grossman RI. MR of wallerian degeneration in the feline visual system: characterization by magnetization transfer rate with histopathologic correlation. *AJNR Am J Neuroradiol* 1994;15:201–212
11. Loevner LA, Grossman RI, McGowan JC, Ramer KN, Cohen JA. Characterization of multiple sclerosis plaques with T1-weighted MR and quantitative magnetization transfer. *AJNR Am J Neuroradiol* 1995;16:1473–1479
12. Kurki TJI, Niemi PT, Lundbom N. Gadolinium-enhanced magnetization transfer contrast imaging of intracranial tumors. *J Magn Reson Imaging* 1992;2:401–406
13. Kurki T, Lundbom N, Hannu K, Valtonen S. MR classification of brain gliomas: value of magnetization transfer and conventional imaging. *Magn Reson Imaging* 1995;13:501–511
14. Wolff SD, Balaban RS. Magnetization transfer contrast (MTC) and tissue water proton relaxation in vivo. *Magn Reson Med* 1989;10: 135–144
15. Eng J, Ceckler TL, Balaban RS. Quantitative magnetization transfer in vivo. *J Magn Reson* 1991;17:304–314
16. Balaban RS, Ceckler TL. Magnetization transfer contrast in magnetic resonance imaging. *Magn Reson Q* 1992;8:116–137

17. Schneider E, Prost RW, Glover GH. Pulsed magnetization transfer versus continuous wave irradiation for tissue contrast enhancement. *J Magn Reson Imaging* 1993;3:417–423
18. Blackband SJ, Hsu E. Magnetization transfer contrast magnetic resonance imaging. In: Gillies RJ, ed. NMR in *Physiology and Biomedicine*. San Diego, Calif: Academic Press; 1994:119–135
19. Hua J, Hurst GC. Analysis of on- and off-resonance magnetization transfer techniques. *J Magn Reson Imaging* 1995;5:113–120
20. Henkelman RM, Huang X, Xiang Q, Stanisz GJ, Swanson SD, Bronskill MJ. Quantitative interpretation of magnetization transfer. *Magn Reson Med* 1993;29:759–766
21. Sepponen RE. Rotating frame and magnetization transfer. In: Stark DD, Bradley WG, eds. *Magnetic Resonance Imaging*. 2nd ed. St Louis, Mo: Mosby-Yearbook; 1992:204–218
22. Hajnal VJ, Baudouin CJ, Oatridge A, Young IR, Bydder GM. Design and implementation of magnetization transfer pulse sequences for clinical use. *J Comput Assist Tomogr* 1992;16:7–18
23. Solomon I. Relaxation processes in a system of two spins. *Phys Rev* 1955;99:559–565
24. Bloembergen N, Morgan LO. Proton relaxation times in paramagnetic solutions: effects of electron spin relaxation. *J Chem Phys* 1966;34:842–850
25. Lauffer RB. Paramagnetic metal complexes as water proton relaxation agents for NMR imaging: theory and design. *Chem Rev* 1987;87:901–927
26. Kang YS, Gore JC, Armmitage IM. Studies of factors affecting the design of NMR contrast agents: manganese is blood as a model system. *Magn Reson Med* 1984;1:396–409
27. Koenig SH, Baglin C, Brown RD III. Magnetic field dependence of solvent proton elevation induced by Gd^{3+} and Mn^{2+} complexes. *Magn Reson Med* 1984;1:496–501
28. Moran PR, Hamilton CA. Near-resonance spin-lock contrast. *Magn Reson Imaging 1995;13: 837–846*
29. Santyr GE, Henkelman RM, Bronskill MJ. Variation in measured transverse relaxation in tissue resulting from spin locking with the CPMG sequence. *J Magn Reson* 1988;79:23–44
30. Santyr GE, Henkelman RM, Bronskill MJ. Spin locking for magnetic resonance imaging with application to human breast. *Magn Reson Med* 1989;12:25–37
31. Santyr GE, Fairbanks EJ, Kelcz F, Sorenson JA. Off-resonance spin locking for MR imaging. *Magn Reson Med* 1994;32:43–51
32. Rommel E, Kimmich R. $T1_\rho$ dispersion imaging and volume-selective $T1_\rho$ dispersion weighted NMR spectroscopy. *Magn Reson Med* 1989;12:390–399
33. Mathur-DeVre R. Biomedical implications of the relaxation behavior of water related to NMR imaging. *Br J Radiol* 1984;57:955–976
34. Koenig SH, Brown RD. Relaxometry and the source of contrast in MRI. In: Gillies RJ, ed. NMR in *Physiology and Biomedicine*. San Diego, Calif: Academic Press; 1994:57–73
35. Sepponen RE, Pohjonen JA, Sipponen JT, et al. A method for $T1_\rho$ imaging. *J Comput Assist Tomogr* 1985;9:1007–1011
36. Mulkern RV, Patz S, Brooks M, et al. Spin-lock techniques and CPMG imaging sequences: a critical appraisal of $T1_\rho$ contrast at 0.15. *Magn Reson Imaging* 1989;7:437–444
37. Jones RA, Southern TE. Improving contrast in rapid imaging sequences with pulsed magnetization transfer contrast. *J Magn Reson* 1992;97:171–176
38. Harrison R. Bronskill MJ, Henkelman RM. Magnetization transfer and T2 relaxation components in tissue. *Magn Reson Med* 1995; 33:490–496